Experimental Investigations of Single Injection in Compensated Silicon at Low Temperatures*

BOB L. GREGORY† AND ANGEL G. JORDAN
Electrical Engineering Department, Carnegie Institute of Technology, Pittsburgh, Pennsylvania
(Received 23 December 1963; revised manuscript received 24 February 1964)

Experimental investigations of the phenomenon of single carrier, space-charge limited injection in silicon at liquid-helium temperatures have been performed in an attempt to validate the model for space-charge limited currents (SCLC) in an insulator with traps. Comparisons between predicted and experimental characteristics were performed on p_+pp_+ devices fabricated by diffusion techniques. Pulse and dc measurements were made to obtain steady-state current-voltage characteristics for the above devices. Modifications were observed in the SCLC characteristics due to field-dependent carrier mobilities, the exact nature of which could be determined from the experimental steady-state characteristics. The density of deep trapping centers in the above material at liquid-helium temperature, corresponding to the compensation, was obtained by measurements of the traps-filled voltage. An independent value for the compensation in the same material was obtained by Hall measurements in the temperature range $20°K<T<77°K$. Transient measurements of the single-carrier current were performed, from which values for the capture probability and capture cross section for the deep trapping center could be obtained. A comparison was made between the capture cross section obtained in this manner and the theoretical prediction of the "giant trap" model.

INTRODUCTION

THE theory of space-charge limited currents (SCLC) in insulators with traps as proposed by Lampert[1] has been employed frequently in recent years to explain the current-voltage characteristics of insulator structures. In some instances, however, uncertainty arose in the interpretation of the insulator characteristics because of apparent disagreement between material parameters obtained from the single injection interpretation and independent material measurements. For example, in CdS, single-carrier SCLC was investigated by Bube[2] in an attempt to correlate the trap density with the traps filled voltage (V_{TFL}) as defined by Lampert. However, his determinations of trap density obtained from measurements of the apparent traps filled voltage differed by as much as three orders of magnitude from independently obtained trap-density values.

This experimental uncertainty in the model for SCLC in insulators with traps prompted the work in this paper. It was observed, originally by Lampert, that the purest insulator in which to test the model would be a high-purity semiconductor at low temperatures (sufficiently low to cause the equilibrium carrier density to be completely negligible). Since the dopant densities in the semiconductor would be known (or could be determined by Hall effect measurements), one should be able to quantitatively compare the predictions of the theoretical model with the experimental characteristics. Other important results expected from investigation of single injection at low temperatures are:

(1) the capture probability, hence capture cross section, of the deep trapping levels present due to compensation could be measured directly by pulse techniques;

(2) the field dependence of the drift mobility could be determined from the SCLC characteristic in the Child's law region;

(3) the injecting nature of contacts at low temperatures could be explored; and

(4) the nature of scattering mechanisms at low temperatures could be better understood by interpreting the field-dependent mobility data.

p_+pp_+ SILICON DEVICES AT LOW TEMPERATURES

As mentioned above, the ideal material in which to examine the model for single-carrier SCLC should be a high-purity semiconductor at low temperatures. In actuality, however, one is limited to germanium or silicon since no other sufficiently pure semiconductors are available. Furthermore, high-purity germanium is unsuitable for these investigations since at low temperatures impact ionization occurs at quite low field strengths,[3,4] destroying its insulating nature. Thus, presently only silicon is suitable for investigating SCLC at low temperature; furthermore, since highest purity silicon is invariably p type due to the presence of boron, p-type material was chosen for the experiment in this work.

As the temperature of a sample is reduced to below the extrinsic range ($T<50°K$ in lightly doped material) the free holes, produced by thermal ionization of noncompensated acceptor centers, recombine with ionized acceptors producing neutral centers. At 4.2°K (liquid-helium temperature) virtually all free holes will have disappeared and N_A-N_D neutral acceptor centers will have appeared. The electrical effect of the compensated

* This work was supported in part by the National Science Foundation.
† Present address: Sandia Corporation, Sandia Base, Albuquerque, New Mexico.
[1] M. A. Lampert, Phys. Rev. **103**, 1648 (1956); J. Appl. Phys. **29**, 1082 (1958).
[2] R. H. Bube, J. Appl. Phys. **33**, 1733 (1962).
[3] N. Sclar and E. Burstein, Phys. Rev. **98**, 1757 (1955).
[4] S. H. Koenig, R. D. Brown, and W. Schillinger, Phys. Rev. **128**, 1668 (1962).

centers at low temperature is to produce trapping levels for injected carriers. The positively charged donor centers would be trapping levels for injected electrons. Similarly, the negatively charged acceptor centers would be traps for injected holes. In this simplified model the impurities consist of N_A shallow acceptors and N_D shallow donors (shallow at room temperature) where $N_A > N_D$. The trapping kinetics for this model depends in large part on the "capture cross section" of the ionized centers. The theoretical considerations which allow this cross section to be determined will be discussed in a later section dealing with the cascade capture process.[5]

To fabricate a single-carrier SCLC device, one must determine which actual contacts exhibit the properties assumed in the model. To reiterate these properties, one contact must be "ohmic" and the other "blocking." At the ohmic contact a large reservoir of holes which can be readily injected into the bulk under forward bias must exist. Such contact is not easily achieved for temperatures in the liquid-helium range. For example, it is known that most metal contacts to silicon create Schottky-type barriers at the metal-semiconductor interface which, though small at room temperature in some cases, are extremely large compared to kT at 4.2°K. Such a barrier would, of course, prevent hole injection at this temperature. A nondegenerate diffused or alloyed p contact would also be unsuitable for use as an injecting contact at these low temperatures since the contact region would merely be an extension of the insulating bulk. However, a degenerate p_+ contact appears to be suitable for the injecting contact at low temperatures since in the degenerate p_+ region there exists a large number of mobile holes which could easily be injected into the insulating region because only a slight barrier exists.

The exact nature of the blocking contact at low temperatures is not so important. Any contact which prevents neutralizing electrons from entering when holes are being injected at the ohmic contact is satisfactory. For this investigation of SCLC the most suitable contact would again be a degenerate p_+ contact since no rectification is desired. No electrons can be injected at this contact at low temperatures regardless of the bias polarity.

The structures in which SCLC was explored at low temperatures were, therefore, p_+pp_+ devices with degenerate p_+ regions. The schematic potential solution for the entire structure in equilibrium is shown in Fig. 1. The metallurgical junctions occur at $X=0$, d in this diagram.

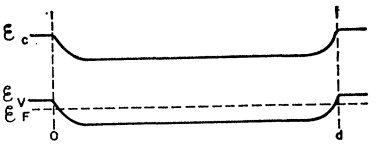

FIG. 1. p_+pp_+ structure in equilibrium.

FIELD-DEPENDENT MOBILITIES AT LOW TEMPERATURES

At temperatures in the liquid-helium range carrier mobilities become field-dependent for values of electric field orders of magnitude smaller than at room temperature. To obtain an explanation for this phenomenon, one must consider the temperature dependence of the mobility. Since at 4.2°K the low-field mobility in lightly doped silicon is more than two orders of magnitude greater than its room-temperature value,[6] the carrier drift velocity at this temperature for a given field strength is likely to greatly exceed the room temperature drift velocity at the same field strength. Therefore the breakdown of the constant mobility assumption, which occurs when the energy given to mobile carriers by the field between collisions is comparable to the equilibrium carrier energy, should occur at greatly reduced electric fields at low temperatures due both to the increased mobility and to the decreased equilibrium carrier energy at these temperatures.

The two principal mechanisms which determine the form of the mobility field dependence are acoustical and optical scattering. Only at very low fields must ionized impurity scattering be considered.[7]

The equation governing the dependence of the mobility μ and electric field E when only acoustical scattering is of importance is

$$\mu = (8/3)^{1/4}(\mu_{LO}c)^{1/2}E^{-1/2}, \tag{1}$$

where μ_{LO} is the acoustical scattering limited zero-field mobility and c is the velocity of sound in the semiconductor.

The field strength at which optical scattering should become important in determining the mobility can be approximated by employing the above equation. If one equates the carrier drift velocity as calculated from this equation to the saturated drift velocity as obtained by equating the carrier kinetic energy to the Raman energy $\mathcal{E}_R$ the following results,

$$(8/3)^{1/4}(\mu_{LO}c)^{1/2}E^{1/2} \cong 1/2(2\mathcal{E}_R/m^*)^{1/2}, \tag{2}$$

where m^* is the density-of-states effective mass.

When the appropriate constants are inserted, it is obtained that in p-type silicon for $E > 50$ V/cm optical scattering should determine the mobility at 4.2°K. This result is surprising when one considers that electric fields near 10^5 V/cm were required at room temperature[8] to cause the carrier drift velocity to approach saturation.

As shall be seen in the following section, the minimum electric field value for which SCLC is observed in the

[5] M. Lax, Phys. Rev. **119**, 1502 (1960).

[6] E. H. Putley and W. H. Mitchell, Proc. Phys. Soc. (London) **72**, 193 (1958).

[7] J. B. Gunn, *Progress in Semiconductors* (John Wiley & Sons, Inc., New York, 1957), Vol. 2, pp. 213–247.

[8] A. C. Prior, Phys. Chem. Solids **12**, 175 (1959).

present compensated silicon devices at low temperatures exceeds the value of 50 V/cm by more than an order of magnitude. One would expect, therefore, that for all the SCLC devices investigated at low-temperature optical scattering is the process determining the carrier mobility.

The simple model for optical scattering, which assumes all carriers are scattered optically upon reaching the threshold energy for optical-phonon emission, allows no carrier energies higher than the threshold energy and predicts drift velocity saturation. When higher carrier energies are allowed, as would be in any realistic model, the drift velocity would not actually saturate. If, for example, the mobility varied as $E^{-\alpha}$, where $\alpha<1$, as some workers have reported, the drift velocity would be proportional to $E^{1-\alpha}$. If one assumes that due to optical scattering the hole mobility μ_P is given by the expression

$$\mu_P=K_0E^{-\alpha}, \tag{3}$$

the constants K_0 and α can be evaluated empirically by comparing the observed Child's law region characteristics to the theoretical Child's law characteristic. When the mobility variation of Eq. (3) is assumed, one can calculate the Child's law characteristic. The resulting equation relating the current density j to the terminal voltage V is

$$j=[(3-\alpha)/(2-\alpha)]^{2-\alpha}(\epsilon K_0)/(2-\alpha)V^{(2-\alpha)}/d^{(3-\alpha)}, \tag{4}$$

where ϵ is the permittivity of the material and d is the device thickness. This equation can be seen to be correct by allowing α to equal zero. In this case the equation reduces to the familiar square-law characteristic for constant mobility.

TRAPPING AT LOW TEMPERATURES

At low temperatures in p_+pp_+ single injection devices, the hole trapping process should involve "giant" traps[5] since Coulombic attraction exists between injected holes and the negatively charged compensated boron atoms. An injected hole would therefore be trapped first in a large orbit excited state of a negative boron center via the emission of a single acoustical or optical phonon. After being trapped in this excited state, the hole would decay to the ground state of the center via a cascade of single-phonon processes.

Whenever carriers are injected into insulators where deep trapping centers exist, the rate at which the carriers are trapped is naturally related to the capture cross section of the centers. In the case of holes injected into p type silicon, the rate at which the carriers are trapped is given by the equation

$$dp/dt=-\bar{B}pN_A^-, \tag{5}$$

where N_A^- is the density of ionized acceptors, p is the density of injected holes, and $\bar{B}$ is the mean-capture probability. $\bar{B}$ is obtained by averaging $B(\mathcal{E})$ over the energy distribution of the injected carriers. The energy-dependent capture probability can be written as

$$B(\mathcal{E})=\sigma(\mathcal{E})(2\mathcal{E}/m^*)^{1/2}, \tag{6}$$

where $\sigma(\mathcal{E})$ is the energy-dependent cross section.

The mean capture probability is therefore seen to be

$$\bar{B}=\langle\sigma(\mathcal{E})(2\mathcal{E}/m^*)^{1/2}\rangle. \tag{7}$$

The experimental values of $\bar{B}$, from which estimates for the capture cross section can be made, can be obtained by comparing the experimental current transients with the analytically derived characteristic. For the condition of slow trapping (the drift transit time $t_d\ll\tau_t$, the trapping time) the following analysis may be employed to obtain the analytical characteristic.

TRANSIENT SCLC IN THE PRESENCE OF SLOW TRAPPING

Carrier flow in a plane parallel insulator with deep traps can be described with four equations: the transport equation, the continuity equation, Poisson's equation, and a rate equation describing the trapping process. If diffusion currents are again neglected, these four equations are as written below:

$$j(X,t)=q\mu_p p(X,t)E(X,t); \tag{8}$$

$$\frac{\partial j(X,t)}{\partial X}=-q\left[\frac{\partial p(X,t)}{\partial t}+\frac{\partial p_t(X,t)}{\partial t}\right]; \tag{9}$$

$$\frac{\partial E(X,t)}{\partial X}=\frac{q}{\epsilon}[p(X,t)+p_t(X,t)+N_D-N_A-n-n_t]; \tag{10}$$

and

$$\frac{\partial p_t(X,t)}{\partial t}=\bar{B}p(X,t)[N_T-p_t(X,t)], \tag{11}$$

where q is the electronic charge, p_t the density of trapped holes, n the density of mobile electrons, n_t the density of trapped electrons, and N_T the density of trapping centers.

In writing Eq. (11), the generation of carriers from the deep traps has been assumed to be negligible. Additional assumptions which appear to be appropriate to the low-temperature situation are:

(1) due to the quasistationary[9] behavior of the carrier flow in the slow trapping situation, both (a) the current divergence $\partial j(X,t)/\partial X$ and (b) displacement currents may be neglected;

(2) at 4.2°K, both n and n_t are negligibly small in p-type material;

(3) since the injected holes are captured on acceptor centers, N_T is equal to N_A in Eq. (11); and

(4) since $t_d\ll\tau_t$, the trap free SCLC solution is assumed to apply at $t=0$.

The simplified equations can be rewritten as

$$j(t)=q\mu_p p(X,t)E(X,t), \tag{12}$$

$$\frac{\partial p(X,t)}{\partial t}=-\frac{\partial p_t(X,t)}{\partial t}, \tag{13}$$

$$\frac{\partial E(X)}{\partial X}=\frac{q}{\epsilon}[p(X,t)+p_t(X,t)+N_D-N_A], \tag{14}$$

$$\frac{\partial p_t(X,t)}{\partial t}=\bar{B}p(X,t)[N_A-p_t(X,t)]. \tag{15}$$

To solve this system of equations for $j(t)$, one proceeds as follows:

(1) relate $p_t(X,t)$ and $p(X,t)$ via Eqs. (13) and (15);

(2) relate $j(t)$ to $p_t(X,t)$ using these results and Eq. (12); and

(3) substitute SCLC initial conditions into the problem obtaining the solution for $j(t)$.

The resulting expression for $j(t)$ is

$$j(t)=J_0\left[\frac{1-[2(2-\alpha)^2(d/X)^{(\alpha-1)/(2-\alpha)}V_{\mathrm{TFL}}/(3-\alpha)V]}{1-[2(2-\alpha)^2(d/X)^{(\alpha-1)/(2-\alpha)}V_{\mathrm{TFL}}/(3-\alpha)V]\exp\bar{B}tN_D\{1-(3-\alpha)(X/d)^{(\alpha-1)/(2-\alpha)}V/2(2-\alpha)^2V_{\mathrm{TFL}}\}}\right]. \tag{16}$$

Equation (16) does not agree completely with the assumptions made in its derivation since it predicts a nondivergenceless current. The divergence is not great, however, since the exponent of the X terms, $(\alpha-1)/(2-\alpha)$, is much less than one for values of α appropriate to the devices of the following section. In fact, for $\alpha=1$, corresponding to drift-velocity saturation, the X dependence disappears altogether yielding a completely divergenceless current. Since the assumptions upon which the present analysis is based are strictly valid only for the case of drift-velocity saturation, the theoretical current transients shall be calculated under this assumption. The difference in form between the characteristics obtained in this manner and the results of an exact solution should not be great since, for values of α reasonably close to one, the X dependence of the current in Eq. (16) is greatly depressed. Hence, by matching the theoretical current transients obtained assuming drift-velocity saturation to the experimental characteristics, one should be able to obtain approximate values for $\bar{B}$ even though the drift velocity has not reached saturation. The theoretical transient characteristic to be employed in these comparisons is obtained by substituting $\alpha=1$ into Eq. (16). This yields

$$j(t)=J_0\left[\frac{1-V_{\mathrm{TFL}}/V}{1-(V_{\mathrm{TFL}}/V)\exp\{\bar{B}tN_C(1-V_{\mathrm{TFL}}/V)\}}\right]. \tag{17}$$

Several limit checks may be performed on this solution to compare it to reality. For example, an obvious limit check is an examination of the behavior of the equation as $t\rightarrow\infty$ for the two cases of $V<V_{\mathrm{TFL}}$ and $V>V_{\mathrm{TFL}}$. For $V<V_{\mathrm{TFL}}$, Eq. (17) predicts that $j(t)\rightarrow 0$ as $t\rightarrow\infty$. This corresponds to the result expected from physical considerations. For the second situation where $V>V_{\mathrm{TFL}}$, the equation predicts that $j(t)\rightarrow J_0(1-V_{\mathrm{TFL}}/V)$, which also corresponds to the expected behavior. An additional check on the equation may be obtained by allowing the density of compensation N_D to become very large. In this case, V_{TFL}/V would be much greater than 1 and $j(t)\rightarrow J_0\exp(-\bar{B}tN_d)$. This simple exponential is the transient characteristic one would expect from physical reasoning for this case, since the density of ionized trapping levels is so large as to remain essentially constant even though carriers are being trapped.[9]

DEVICE CONSTRUCTION AND EVALUATION

The degenerate p_+ contacts were formed by comparatively low-temperature boron diffusions. For the temperatures employed (900–950°K) the surface concentration of boron exceeded 10^{20} cm^{-3} as was observed from sheet resistivity and junction depth measurements on identically diffused n-type wafers.[10] These measurements indicated junction depths of approximately 1 μ in addition to the above value of surface concentration.

Two techniques were employed to fabricate single injection devices from the diffused wafers. Circular devices with areas of approximately 10^{-2} cm^2 were obtained by masking and etching. Rectangular devices of comparable area were made by scribing and breaking the diffused samples. Leads were attached to the above devices by thermocompression bonding aluminum wire.

To obtain measurements at 4.2°K on these devices, a shielded, light-tight cryostat was employed. To obtain the necessary low temperature, the cryostat was inserted into the liquid-helium chamber of a double-walled transport Dewar.

To measure the steady-state current-voltage characteristics over the relatively large range of currents observed in SCLC devices, several techniques were employed. Below 1 mA, dc measurements could be taken without appreciable heating. Consequently currents between 10^{-9} and 10^{-3} A were observed using dc schemes. Point by point measurements were made in some cases using a well-shielded circuit employing a

[9] A. Many and G. Rakavy, Phys. Rev. **126**, 1980 (1962).
[10] G. Backenstoss, Bell System Tech. J. **37**, 699 (1958).

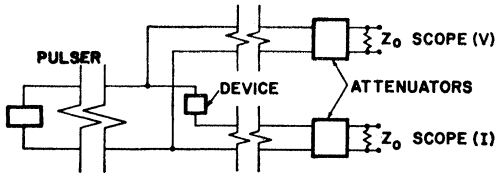

FIG. 2. Pulse measurement circuit.

precision decade resistance box to sense the current. In many instances, however, the dc data were obtained using an oscilloscope as an X-Y plotter. This procedure speeded up the data taking process considerably while still allowing accuracy within the range required. In some cases the device characteristics were observed on a curve tracer when high accuracy was not needed.

For currents greater than 10^{-3} A where heating would prevent dc measurements, the steady-state current-voltage characteristics were obtained using repetitive submicrosecond pulses. The pulse measurement setup, as shown in Fig. 2, differed slightly from the dc setup since to prevent reflections the transmission lines were matched with their characteristic impedance Z_0 at all terminations. The pulse duration in these measurements varied between 100 and 300 nsec. The repetition rate was approximately 150–350 pulses per second. A fast rise-time oscilloscope (Tektronix 555) was used to observe the pulses in all cases.

The single-shot pulse measurements, used to approximate the trap-free SCLC, were taken with the same circuit as shown in Fig. 2. A single-shot measurement was made by pulsing the device once after it had been thermally cycled from 300 to 4.2°K. The oscilloscope traces corresponding to the single-shot voltage and current pulses were recorded on high speed film, providing records from which the data could later be taken and analyzed.

EXPERIMENTAL CURRENT-VOLTAGE CHARACTERISTICS

The experimental steady-state current-voltage characteristics as obtained at 4.2°K for p_+pp_+ silicon devices exhibited the structure one would expect for SCLC in an insulator with deep trapping levels. In Fig. 3 the steady-state characteristic has been plotted for device II. This characteristic, which is typical of all the devices tested, clearly shows the presence of a traps-filled voltage, at which point the current increases steeply with voltage. When the traps-filled voltage is measured for this device and for the others constructed from the same material, the values tabulated in Table I are obtained. If the trap density were uniform, as was previously assumed above, a d^2 dependence would be observed in V_{TFL}. By plotting $\log V_{\mathrm{TFL}}$ versus $\log d$, where d is the minimum thickness, a straight line of slope two would connect the measurements for the various devices for this dependence. In Fig. 4 this plot is shown including the possible errors in device thickness

TABLE I. Traps-filled voltage values and the corresponding minimum thicknesses for several devices.

Device	Minimum thickness (cm)	V_{TFL} (V)
O	7.7×10^{-3}	31
II	6.8×10^{-3}	25
III	8.2×10^{-3}	36
IV	9.0×10^{-3}	44
VII	1.1×10^{-2}	57
VIII	7.2×10^{-3}	25
IX	8.2×10^{-3}	32.5

measurements ($\pm5\,\mu$). The experimental points lie very close to the predicted slope-two line. The traps-filled voltage value obtained for each device allows a determination of the trap density in the device. When this is done for all the devices in Table I, a mean trap density of 6.1×10^{12} cm^{-3} is obtained. The maximum deviation from this value in the devices measured was approximately 10%.

From the steady-state curve in Fig. 3 the form of the current-voltage characteristic in the Child's law region can be determined. However, the limited data in this region make the determination, with any degree of accuracy, rather difficult. To decrease the possible error associated with fitting the Child's law region, single-shot pulse measurements can be made, to approximate the trap-free characteristic. These measurements, as taken for the device in Fig. 3 are plotted as the boxed data points on the same curve. The agreement between the steady-state and single-shot curves in this figure indicates the usefulness of the single-shot measurements in obtaining an extension of the Child's law region.

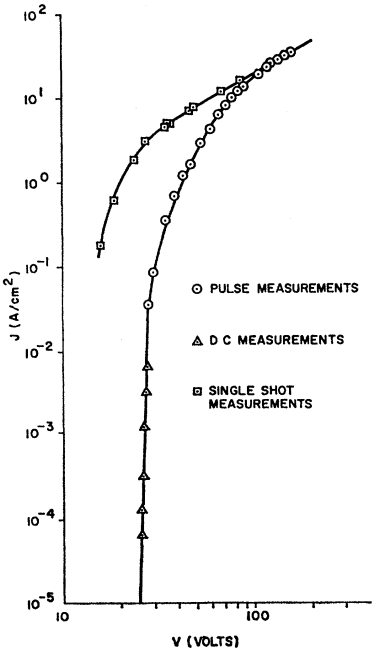

FIG. 3. Steady-state and single-shot pulse measurements for device II.

By measuring the slope m of the characteristic in the extended Child's law region one can obtain from Eq. (4) $m=(2-\alpha)$. For the devices analyzed a mean value of 0.64 was obtained for α.

From the value of K_0 and the slope of the characteristic in the Child's law region, the field-dependent carrier mobility at low temperatures can be determined. In the range of applied fields 3×10^3 V/cm$<E<3\times10^4$ V/cm the relationship between mobility and electric field was found to be

$$\mu_P(E)\approx(2.6\pm1.4)\times10^5E^{-(0.64\pm0.04)}\ \text{cm}^2/\text{Vsec}. \quad (18)$$

The steeply rising region of the steady-state characteristic following V_{TFL} can be obtained analytically for the two cases of constant mobility or constant drift velocity. However, for the more general situation where the mobility is field-dependent but the drift velocity not saturated, no analytical solution can be obtained. To obtain the characteristic for this case a numerical solution would be necessary. The effort required to obtain this solution would not be justifiable since little additional information would result. However, the basic fact about the steeply rising region is that any model, which assumes the onset of SCLC after a traps-filled voltage, predicts an extremely steep characteristic regardless of the applicable $\mu(E)$ function. This prediction is most definitely verified by the previous experimental characteristics.

CAPTURE PROBABILITY AND CAPTURE CROSS-SECTION MEASUREMENTS

The mean capture probability,[5] $\bar{B}$, can be obtained from the same single-shot pulse measurements that were utilized to obtain the extended Child's law region of Fig. 3. Two pulse recordings, typical of those employed to obtain $\bar{B}$, are shown in Fig. 5 as photographed from the oscilloscope display.

There are two ways in which one can obtain $\bar{B}$ from the single-shot current response. One can (a) match the theoretical transient characteristic [Eq. (17)] to the experimental pulse, or (b) estimate the initial time constant of the decaying current pulse and compare it to the theoretical initial time constant.

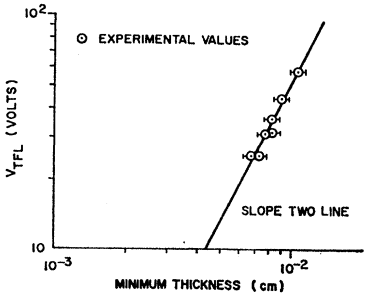

FIG. 4. Thickness dependence of V_{TFL}.

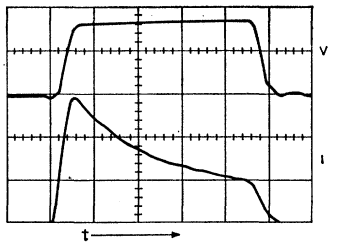

FIG. 5. Typical voltage and current transients obtained by single-shot pulse measurements. Scales: $t=40\times10^{-9}$ sec/major division: $V=25$ V/major division; $I=20$ mA/major division.

Equation (17) is rewritten for clarity as

$$j(t)=J_0\frac{1-V_{\text{TFL}}/V}{1-(V_{\text{TFL}}/V)\exp\bar{B}N_d(1-V/V_{\text{TFL}})t}.$$

It is seen to contain the parameters J_0 and $\bar{B}$ in addition to the previously determined constants N_d and V_{TFL}.

Some uncertainty exists as to where $t=0$ should be situated on the experimental pulse in order to cause it to correspond to the analytical characteristic of Eq. (17). Due to the accumulated rise time of the generator, oscilloscope, and measuring circuit there exists an uncertainty of approximately 20 nsec. Two alternative methods of matching the theoretical and experimental characteristics present themselves. One can assume

(a) that the beginning of the current pulse, $i(t)$, through the device corresponds to approximately 20×10^{-9} sec before the peak of the $i(t)$ pulse, or

(b) that negligible trapping occurs prior to the peak of the $i(t)$ pulse in which case this point would correspond to $t=0$ in the theoretical characteristic.

Case (a) involved matching the theoretical and experimental characteristics at two points to allow determination of both J_0 and $\bar{B}$ for each pulse. This technique was therefore called a "two-point fit." Case (b) involved matching the characteristics at only one point since J_0 was known. This case was called a "one-point fit." In Fig. 6 the experimental pulse responses of two typical devices are plotted as circled points. Both one- and two-point fits were performed for these units and the results are also shown. It was observed that for these and other pulses the one-point fit tended to more closely approximate the experimental results. This would indicate that no appreciable trap filling occurred for most pulses before the peak of the experimental characteristic.

The second general technique for calculating the mean capture probability from the experimental data was to relate the initial time constant τ_{TO} for decay of the current pulse to $\bar{B}$. Since at $t=0$ the density of trapping centers is approximately equal to N_D, one obtains that

$$B=1/\tau_{\text{TO}}N_D, \quad (19)$$

where τ_{TO} may be obtained by estimating the initial

TABLE II. Capture probability and capture cross section values for negatively ionized boron centers in compensated silicon at 4.2°K.

Device	Method	$\bar{B}$ (cm³/sec)	$\sigma(\mathcal{E}_d)$ (cm²)	$\bar{E}$ (V/cm)
II	Initial slope	1.0×10^{-6}	2.0×10^{-13}	3.5×10^{3}
II	Initial slope	2.2×10^{-6}	4.0×10^{-13}	4.7×10^{3}
III	Initial slope	3.6×10^{-6}	6.9×10^{-13}	4.1×10^{3}
III	Initial slope	2.0×10^{-6}	4.9×10^{-13}	2.1×10^{3}
III	Initial slope	2.8×10^{-6}	6.1×10^{-13}	2.9×10^{3}
III	2-Point fit	3.2×10^{-6}	5.0×10^{-13}	7.1×10^{3}
III	1-Point fit	2.05×10^{-6}	3.4×10^{-13}	7.1×10^{3}
III	2-Point fit	1.6×10^{-5}	2.9×10^{-12}	4.8×10^{3}
III	1-Point fit	3.0×10^{-6}	5.5×10^{-13}	4.8×10^{3}
VII	Initial slope	4.0×10^{-6}	7.3×10^{-13}	4.9×10^{3}
VII	2-Point fit	6.0×10^{-6}	1.1×10^{-12}	4.9×10^{3}
IX	Initial slope	$(1.75\text{–}3.5)\times10^{-6}$	$(3.6\text{–}7.3)\times10^{-13}$	3.3×10^{3}
IX	Initial slope	1.5×10^{-6}	3.3×10^{-13}	2.7×10^{3}
IX	2-Point fit	3.8×10^{-6}	7.2×10^{-13}	4.4×10^{3}
IX	1-Point fit	2.2×10^{-6}	4.2×10^{-13}	4.4×10^{3}
IX	1-Point fit	1.4×10^{-6}	2.1×10^{-13}	8.3×10^{3}
IX	1-Point fit	1.4×10^{-6}	2.3×10^{-13}	6.6×10^{3}

slope of $i(t)$ on a semilogarithmic plot. For this reason this technique was called the "initial slope" method.

In Table II the values of $\bar{B}$ obtained by these three methods for several devices have been tabulated. The average electric field (V/d) is shown for each measurement. Because of the large scatter of the experimental results, no field dependence could be detected in the B measurements. By averaging the values for each of the techniques one obtains: (a) $\bar{B}=2.4\times10^{-6}$ from initial slope measurements, (b) $\bar{B}=2.0\times10^{-6}$ from one-point fitting of the theoretical characteristic, and (c) $\bar{B}=7.2\times10^{-6}$ from two-point fitting of the theoretical characteristic.

Since the value of $\bar{B}$ given in (c) does not agree well with (a) or (b) the value of $\bar{B}=2.2\times10^{-6}$ cm³/sec is chosen as the most probable.

In order to calculate a meaningful capture cross section for the trapping levels from the $\bar{B}$ value given above, one must know not only the energy distribution

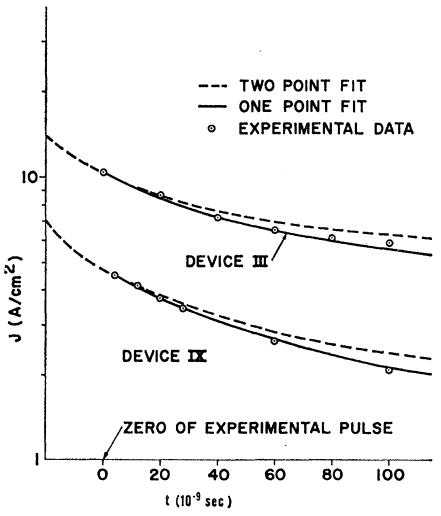

FIG. 6. Theoretical and experimental transient characteristics for devices III and IX.

of the carriers but also the energy dependence of the capture cross section since $\bar{B}$ is given by Eq. (7). However, in the high-field case certain assumptions about the energy distribution of the carriers can be made which simplify the relationship between $\bar{B}$ and σ. For this case, because of the heating effect of the electric field on the carriers, optical mode scattering is the dominant energy-loss mechanism. If one assumes that the component of the carrier energy contributed by the field between optical collisions is much greater than the carrier energy remaining after a collision, the average carrier energy will be given by

$$\mathcal{E}_d=(1/2)m^*v_d^2, \tag{20}$$

where v_d is the drift velocity. If one also assumes that few carriers have energy is excess of $\mathcal{E}_R$, Eq. (7) simplifies to

$$\bar{B}=\sigma(\mathcal{E}_d)(2\mathcal{E}_d/m^*)^{1/2}. \tag{21}$$

Replacing the quantity

$$(2\mathcal{E}_d/m^*)^{1/2}$$

by its equivalent

$$K_0E^{1-\alpha},$$

one obtains from (21) the simple expression

$$\sigma(\mathcal{E}_d)=\bar{B}/K_0E^{1-\alpha}. \tag{22}$$

The values of $\sigma(\mathcal{E}_d)$ calculated by applying Eq. (22) to the values of $\bar{B}$ in Table II have been included in this table. The mean value of σ as taken from the initial slope and one point fit calculations is

$$\bar{\sigma}\approx4.4\times10^{13}\text{ cm}^2.$$

This value applies for a mean electric field of 4.6×10^3 V/cm.

The above experimental capture cross section can be compared to the prediction of the giant trap model by calculating the theoretical value of the energy-dependent capture cross section via relationships derived by Lax.[5] For the case of trapping via optical-phonon-emission Lax's theory predicts values for the capture cross section in the range

$$1.4\times10^{-13}\text{ cm}^2<\sigma<5.6\times10^{-13}\text{ cm}^2,$$

when constants appropriate to silicon at 4.2°K are inserted. In Appendix A this calculation is performed in detail. One observes from this range of values of σ that the previously obtained experimental value of 4.4×10^{-13} cm² is indeed reasonable.

HALL-EFFECT DETERMINATION OF COMPENSATION

Although the low-temperature single injection experiments above provided values for the compensation via traps-filled voltage measurements, it was felt that a separate determination of the compensation by a more

conventional technique was necessary for corroboration. For this purpose Hall-effect measurements were performed over the temperature range $25°K<T<77°K$, whereby one could obtain both the majority dopant depth and degree of compensation.

The temperature-dependent hole concentration in p-type silicon at low temperatures is known to be given by the expression

$$p=\left(\frac{2\pi m^*T}{h^2}\right)^{3/2}\frac{(N_A-N_D)}{2N_D}\exp(-\mathcal{E}_A/kT), \quad (23)$$

where $\mathcal{E}_A$ is the acceptor activation energy.

To obtain the compensation N_D from the Hall data one observes that it is necessary to plot the quantity $\ln(pT^{-3/2})$ versus $1/T$. Over the region of applicability of Eq. (23) this plot yields a straight line of slope $-\mathcal{E}_A/k$ from which one obtains the acceptor activation energy. Furthermore, if the linear region of the plot is extrapolated to the $1/T=0$ axis, the intercept allows a determination of the quantity $(N_A-N_D)/N_D$. Since (N_A-N_D) can be obtained from Hall measurements in the exhaustion region, a measurement of the intercept readily yields the compensation N_D.

For three Hall samples this plot is shown in Fig. 7. Device I–II was constructed of material diffused simultaneously with that of the single injection devices previously considered. Device III–II and III–III were fabricated from the results of a separate diffusion performed under near identical circumstances on the same starting material. The results for these three samples are tabulated in Table III. One observes that the results for devices III–II and III–III are quite similar. However, the degree of compensation in these two devices differs by a factor of 2 from that measured for device I–II. This result supports the hypothesis that most of the compensation present in the devices was created during the diffusion step. The compensation observed in device I–II (6.6×10^{12} cm^{-3}) was quite close to the average value of 6.1×10^{12} cm^{-3} obtained from the previous V_{TFL} measurements. This degree of agreement between the two values is quite good, especially since finding N_D in the Hall experiment involves extrapolating the $pT^{-3/2}$ curve over a region as extensive as the straight line region itself.

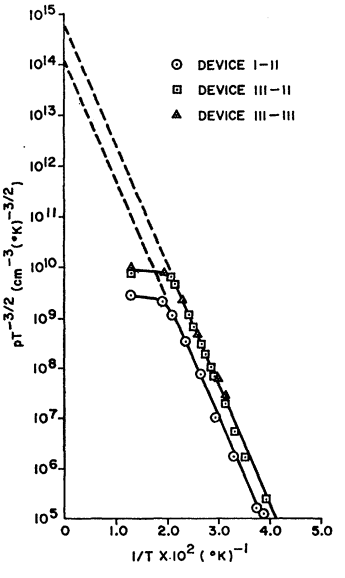

FIG. 7. $pT^{-3/2}$ versus $1/T\times10^2$ for Hall devices I–II, III–II and III–III.

TABLE III. Impurity concentrations and acceptor depth as determined by Hall-effect measurements.

Device	Type	E_D (eV)	(N_A-N_D) (cm^{-3})	N_D (cm^{-3})	N_A (cm^{-3})
I–II	p	47×10^{-3}	1.7×10^{12}	6.6×10^{12}	8.3×10^{12}
III–II	p	47×10^{-3}	5.4×10^{12}	3.9×10^{12}	9.3×10^{12}
III–III	p	47×10^{-3}	5.6×10^{12}	3.8×10^{12}	9.4×10^{12}

The activation energy $\mathcal{E}_A$ of the acceptor center, corresponding to the trapping depth at 4.2°K, was approximately 0.047 eV for all devices. This value is known to correspond to boron in silicon.[11]

DISCUSSION AND CONCLUSIONS

In considering the model for p_+pp_+ devices at liquid-helium temperature a threshold voltage for injection is found to exist. This threshold is due to the barrier created at the p_+p junction by holes trapped near the junction in the equilibrium situation. The exact form of the Child's law region at low temperatures is dependent on the mobility-electric field relationship appropriate to the range of fields employed. For a mobility dependence as given by expression (3) the general Child's law relationship has the form of Eq. (4).

In order to relate the observed single-shot current pulses to the trapping capture probability, an approximate solution has been obtained for the current as a function of time under the conditions of slow trapping. This solution is as indicated by Eq. (17) if the current flow is assumed divergenceless. This assumption is strictly valid only for the case of drift-velocity saturation; therefore for $\alpha<1$ in expression (3) a slight disparity between the analytical expression for the current density and the actual characteristics is expected to exist.

The experimental results indicate that the SCLC model, modified to include the appropriate field-dependent mobility, applies for p-type silicon at 4.2°K. The steady-state current-voltage characteristics observed at this temperature correspond in form and magnitude to the predictions of the SCLS model for an insulator with a deep trap density of 6.1×10^{12} cm^{-3}. By single-shot pulse techniques the experimental Child's law regions could be extended to lower applied voltages.

[11] N. B. Hannay, *Semiconductors* (Reinhold Publishing Corporation, New York, 1960), p. 472.

Based on these extended power law regions the appropriate form of Child's law was found to be $j\sim V^{1.36}$. The mobility implied by the characteristic in this region was

$$\mu_P\simeq(2.6\pm1.4)10^5E^{-(0.64\pm0.04)}\ \text{cm}^2/\text{Vsec}.$$

A trap density of 6.1×10^{12} cm^{-3} was obtained by trap-filled voltage measurements and it should correspond to the compensation in the material. This compensation was measured separately by a Hall-effect experiment over the temperature range $25°\text{K}<T<77°\text{K}$ and found to be approximately 6.6×10^{12} cm^{-3}, which agrees reasonably well with the value above. Also from the Hall experiment a value for the acceptor level of 0.047 eV was obtained, which agrees reasonably well with the expected value for boron in silicon.

Experimental values for the capture probability and capture cross section were obtained by fitting the analytical characteristic for the current density to the observed pulses. The average experimental value for the mean capture probability was $\bar{B}=2.2\times10^{-6}$ cm^3 sec^{-1}. If all the carriers are assumed to have the same velocity, this value could be converted to a corresponding one for capture cross section. The latter, as obtained by averaging the values obtained from the many experimental measurements of $\bar{B}$, was $\bar{\sigma}=4.4\times10^{-13}$ cm^2. The theoretical value of σ, as predicted by the giant trap model, was calculated for the case of trapping via optical-phonon emission. A value of σ in the range $1.4\times10^{-13}<\sigma<5.6\times10^{-13}$ cm^2 resulted. The agreement between experimental and theoretical values is again quite reasonable.

APPENDIX A

For the case of trapping via optical-phonon emission, Eq. (A1) relates σ and $\mathcal{E}$, the carrier energy. This equation is

$$\sigma(\mathcal{E})=\frac{\pi^2}{8}\frac{w}{l_c}\frac{q^2}{\epsilon}\left(\frac{q^2}{\epsilon\hbar\omega}\right)^2\times\frac{\lambda}{1-\exp(-\lambda)}\frac{P(\hbar\omega-\mathcal{E})}{(1-\mathcal{E}/\hbar\omega)^{5/2}}(1+a\bar{y})^{1/2},\quad\text{(A1)}$$

where the various quantities are defined as: $\hbar\omega=\mathcal{E}_r$ the Raman energy (0.063 eV for silicon), $\lambda=\hbar\omega/kT$, $P(\hbar\omega-\mathcal{E})=$the "sticking probability," $a=((\hbar\omega-\mathcal{E})/\hbar\omega)$, $\bar{y}\approx0.85$, $l_c=$the mean free path for acoustical scattering, and $w=$a constant which relates the strength of coupling of the carriers to the optical modes to the strength of coupling to acoustical modes.[12] After substituting the appropriate values of the above terms for silicon at 4.2°K into Eq. (A1) one obtains that

$$\sigma=8.5\times10^{-16}w/l_c,\quad\text{(A2)}$$

when $E=4.6\times10^3$ V/cm.

Choosing the pure acoustical scattering mobility at 4.2°K to be approximately 10^6 cm^2/Vsec for p-type silicon, as the results of Putley and Mitchell[6] would indicate, l_c would be approximately 6×10^{-4} cm. Therefore at 4.2°K

$$\sigma\approx1.4\times10^{-13}(w)\ \text{cm}^2.\quad\text{(A3)}$$

The value of w can be estimated based on the existing data for mobility versus temperature in the range $100°\text{K}<T<300°\text{K}$.[6] It would appear that $1<w<4$ is applicable for p-type silicon.

For this range of w one finds that

$$1.4\times10^{-13}\ \text{cm}^2<\sigma<5.6\times10^{-13}\ \text{cm}^2.$$

[12] C. Herring, Bell System Tech. J. 34, 237 (1955).